Body-force modeling for aerodynamic analysis of air intake – fan interactions

William Thollet
Airbus Operations SAS, Toulouse, France and
Département Aérodynamique Energétique et Propulsion,
ISAE – Supaero, Toulouse, France
Guillaume Dufour and Xavier Carbonneau
Département Aérodynamique Energétique et Propulsion,
ISAE – Supaero, Toulouse, France, and
Florian Blanc
Airbus Operations SAS, Toulouse, France

Abstract

Purpose – The purpose of this paper is to explore a methodology that allows to represent turbomachinery rotating parts by replacing the blades with a body force field. The objective is to capture interactions between a fan and an air intake at reduced cost, as compared to full annulus unsteady computations.

Design/methodology/approach – The blade effects on the flow are taken into account by adding source terms to the Navier-Stokes equations. These source terms give the proper amount of flow turning, entropy, and blockage to the flow. Two different approaches are compared: the source terms can be computed using an analytic model, or they can directly be extracted from RANS computations with the blade's geometry.

Findings – The methodology is first applied to an isolated rotor test case, which allows to show that blockage effects have a strong impact on the performance of the rotor. It is also found that the analytic body force model underestimates the mass flow in the blade row for choked conditions. Finally, the body force approach is used to capture the coupling between a fan and an air intake at high angle of attacks. A comparison with full annulus unsteady computations shows that the model adequately captures the potential effects of the fan on the air intake.

Originality/value – To the authors' knowledge, it is the first time that the analytic model used in this paper is combined with the blockage source terms. Furthermore, the capability of the model to deal with flows in choked conditions was never assessed.

Keywords Fan, Interaction, Distortion, Airframe, Body force, Source terms

Paper type Research paper

Nomenclature

x	axial direction	κ	blade camber angle
r	spanwise direction	h	blade to blade staggered spacing
θ	tangential direction	Ω	blade rotational speed
m	meridional direction	$\overrightarrow{f}$	body force vector
b	blade blockage factor	$\overrightarrow{v}$	absolute velocity vector

This study was founded by Airbus Operation SAS and ANRT (Association Nationale de la Recherche et de la Technologie). The authors would like to thank Marc Julian and Thierry Surply, for their precious advice and lectures on the functioning of the air-intake aerodynamics.

$\vec{w}$	relative velocity vector	M_r	relative mach number
h_t	stagnation enthalpy	δ	flow deviation
e_t	stagnation energy	Q^*	normalized mass flow
P	static pressure		

1. Introduction

Some of the main challenges for the next generation of commercial aircraft are the reduction of fuel burn, engine emissions, and noise. One way to achieve this is to seek higher bypass ratio for turbofan engines, which increases propulsive efficiency (Owens *et al.*, 1990) and potentially allows to reduce far field and cabin noise (Hall and Crichton, 2007). To limit the drag and weight increase of the nacelle, new options must be considered during the engine integration process, such as the reduction of the length to diameter ratio (L/D) of the air intake (Figure 1).

However, shortening the inlet leads to new or increased aerodynamic interactions between the engine fan and the airframe, acting on the air intake performance and possibly leading to fan performance deterioration (Larkin and Schweiger, 1992). While an accurate prediction of these interactions can be obtained with a full annulus unsteady CFD approach (Yao *et al.*, 2010; Fidalgo *et al.*, 2012), the cost and the complexity of this method are prohibitive for daily design loops.

In this context, this study focusses on a particular type of turbomachinery modeling known as "body force modeling," in which the blades are replaced by a body force field producing the same amount of flow turning and entropy. One method to build the force field is to write an analytic model for the blade force. Another method is to extract the body forces from a RANS computation of the fan, as in Kiwada (2008). In the second approach, a specific term is often included into the RANS equations in addition to the body forces to account for the blockage effects of the blade geometry. However, this term is in general not included in analytic approaches, and its impact has never been directly assessed. The objectives of the present contribution are thus to:

(1) determine the effect of the blockage term in the body force approach;

(2) assess and compare an analytic model and the RANS extraction method; and

(3) apply these methods on an air intake test case.

First, body force modeling concepts and main applications in the literature are discussed. Then, the analytic model and the RANS-extraction methodology adopted for

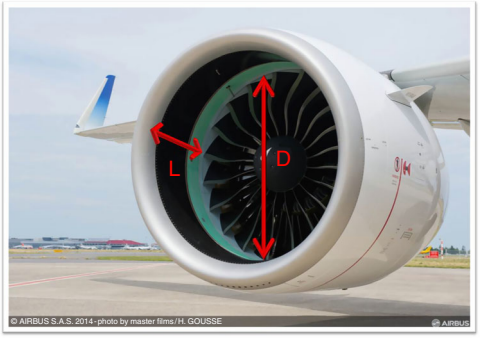

Figure 1.
Illustration of a modern high bypass ratio engine (PW1000G, A320 NEO)

this study are described. Both approaches are first applied to an isolated single-passage rotor test case, then the model is applied to an air intake case and compared to results obtained with full annulus unsteady computations.

2. Body force modeling

2.1 Concepts and limitations

The body force concept was first introduced by Marble (1964), who proposed to represent the effect of a blade row on the flow by external forces, and derived thermodynamic relations linking these forces to flow deviation and entropy elevation. This concept has been widely used in throughflow applications such as the streamline curvature (SLC) method, and more recently in 3D CFD (Hsiao *et al.*, 2001). In these applications, the blade force is represented by source terms in the RANS equations.

The main advantage of this approach is that the number of mesh cells is reduced as compared to classical computations with the blades, since the boundary layers on the blade walls do not have to be resolved. In addition, the effect of the blades on the flow is redistributed in the tangential direction, allowing to handle cases with distortion with steady computations, whereas the presence of discrete blades would require to perform an unsteady computation to correctly capture the wakes. Unlike the actuator disk method, the source terms are active in the whole volume swept by the blades (Figure 2), which allows to capture effects occurring within the blade row such as mass flow redistribution.

One limitation of this approach, however, is that it does not naturally account for the section variation due to the presence of solid blades in the channel as the whole volume swept by the blades is meshed. The effect of blockage can be of particular importance if the flow is transsonic, as it drives the maximum mass flow through the blade row when a sonic throat appears. This blockage has two components: the metal blockage, due to the thickness of the blades, and the aerodynamic blockage due to the boundary layers on the blade walls. Blockage effects can be taken into account with a section reduction factor on the left hand side of the RANS equations (Simon, 2007; Kiwada, 2008), but it involves either an artificial reduction of the surfaces and volume of each cell in the blade row, or a modification of the conservative variables. A more convenient solution is to add a source term on the right hand side of the RANS equations (Kottapalli, 2013). It should nevertheless be kept in mind that this choice involves the addition of a source term to the continuity equation, which could lead to non-conservative mass flow if the blockage term is computed inaccurately. This is further discussed in Section 3.2.

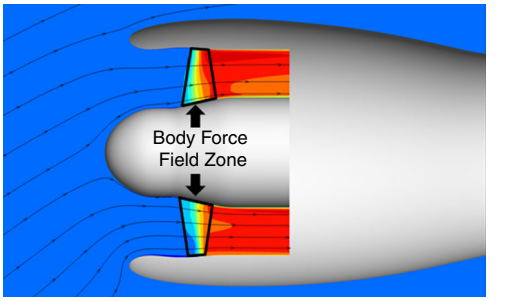

Note: Side view, contours of total pressure

Figure 2.
Illustration of the body force methodology applied to a 3D air intake case

2.2 Implementation

In body force modeling, the blade effects are taken into account by adding a source term on the right hand side of the RANS equations. The following equations are then resolved (viscous flux and heat transfer are omitted for clarity):

$$\frac{\partial \rho}{\partial t} + div\left(\rho \vec{v}\right) = -\frac{1}{b}\left(\rho \vec{v} \cdot \vec{\nabla} b\right) \tag{1}$$

$$\frac{\partial \rho \vec{v}}{\partial t} + div\left(\rho \vec{v}\, \vec{v}^{t}\right) + \vec{\nabla} P = \rho \vec{f} - \frac{1}{b}\left(\rho \vec{v} \cdot \vec{\nabla} b\right) \vec{v} \tag{2}$$

$$\frac{\partial \rho e_t}{\partial t} + div\left(\rho h_t \vec{v}\right) = \rho \Omega r f_\theta - \frac{1}{b}\left(\rho h_t \vec{v} \cdot \vec{\nabla} b\right) \tag{3}$$

where b is the blockage factor defined in Figure 3. With this definition, aerodynamic blockage is not taken into account, which is deemed acceptable for a first order approximation. $\vec{f}$ f is the body force vector, either determined using an analytic model, or extracted from a single passage RANS computation with the fan geometry. These two approaches are described in the next sections.

2.2.1 RANS-extracted body force field. In classical throughflow modeling, the body forces evaluation is mostly based on correlations coming from experimental data and general experience. In several studies conducted at the MIT, body forces extracted from RANS single passage computations are imposed in a 3D Euler solver for stall inception and performance prediction in the stall region (Kiwada, 2008; Benneke, 2009; Patel, 2009). To achieve this, the body forces are extrapolated outside the range of stable operating points obtained with steady state CFD, using results from SLC computations for instance. While the results obtained with this method are promising, it has not been applied to cases with distortion patterns such as those encountered in an air intake at high angle of attack (AOA).

The present study uses the procedure described in Kiwada's (2008) work to extract the body forces. First, a 3D computation is performed on a single channel with the blade geometry. The resulting flow is pitch averaged on a 2D meridional grid. Equation (4), which is the axisymmetric form of the Euler equations, is then applied to the resulting axisymmetric flow, to obtain the source term S defined in Equation (7). Spatial derivatives

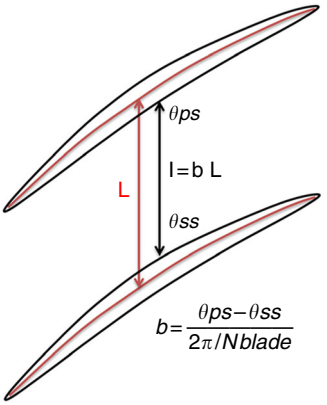

Figure 3.
Illustration of the blade metal blockage parameter

are evaluated using second order centered differences on the meridional grid cell centers. This source term contains both the blockage effect and the blade forces. Noting that all the blockage source terms can be deduced from the source term in the continuity equation, it is then possible to deduce the body force vector $\overrightarrow{f}$ on each meridional cell. A disadvantage of this method, as compared to others where the body forces are extracted from the blades pressure and friction repartition (Peters *et al.*, 2014; Defoe *et al.*, 2010), is that the resulting body forces include the endwall viscous effects. This means that performing a viscous computation with these body forces will result in taking into account the viscous effects on the end walls in the blade region twice:

$$\frac{\partial \overline{F}}{\partial x}+\frac{\partial \overline{H}}{\partial r}=S, \tag{4}$$

where:

$$F=\begin{pmatrix} r\rho V_x \\ r\rho V_x^2+rP \\ r\rho V_x V_r \\ r\rho V_x V_\theta \end{pmatrix} \tag{5}$$

$$H=\begin{pmatrix} r\rho V_r \\ r\rho V_x V_r \\ r\rho V_r^2+rP \\ r\rho V_r V_\theta \end{pmatrix} \tag{6}$$

$$S=\begin{pmatrix} -r\frac{1}{b}\left(\rho\overrightarrow{v}\cdot\overrightarrow{\nabla}b\right) \\ rf_x-r\frac{1}{b}V_x\left(\rho\overrightarrow{v}\cdot\overrightarrow{\nabla}b\right) \\ P+\rho V_\theta^2+rf_r-r\frac{1}{b}V_r\left(\rho\overrightarrow{v}\cdot\overrightarrow{\nabla}b\right) \\ \rho V r V_\theta+rf_\theta-r\frac{1}{b}V_\theta\left(\rho\overrightarrow{v}\cdot\overrightarrow{\nabla}b\right) \end{pmatrix} \tag{7}$$

Repeating this procedure along an operating line allows to obtain a body force field for each operating point.

2.2.2 Analytic model. The analytic body force model chosen for this work was developed by Gong (1998), who successfully used it to reproduce the unsteady behavior of a compressor in the stall region of the map. Later, the model was applied to an air intake case (Hsiao *et al.*, 2001), the focus being put on the effect of the fan on inlet flow separation. In another study, a modified version of this model was used to study the generation and the propagation of fan rotor shock noise in a serpentine inlet (Defoe *et al.*, 2010). More recently, Gong's model was applied with success to short inlet cases to capture inlet-fan and fan-exhaust interactions (Peters *et al.*, 2014). The main limitation in this last study is that the blockage is only taken into account by modifying the value of the blade forces.

The current implementation consists of Gong's original model, with the modifications proposed by Peters *et al.* (2014) for the loss coefficient. In this model, the blade force is divided into two components that depend on both local flow conditions and blade geometry: one orthogonal to the relative flow field and responsible for flow turning, and one parallel to the relative flow, which generates losses. The expression for these components are detailed in Equations (8) and (9):

$$f_n = \frac{1}{\rho}\frac{\partial P}{\partial x}\sin\kappa + \frac{K_n(x,r)}{h}W^2\frac{1}{2}\sin(2\delta) \tag{8}$$

$$f_p = \frac{K_p}{h}W^2$$

$$K_p = K_{p0} + K_{p1} \times M_r + K_{p2} \times M_r^2 \tag{9}$$

where κ is the blade camber angle, W the relative velocity norm, h the blade to blade staggered spacing, and δ the flow deviation $\beta - \kappa$, with β the relative flow angle. More details can be found in Gong (1998) (Figure 4).

Both components rely on a calibration coefficient (K_n, K_p) that can be computed from experimental data and correlations (Gong, 1998), or retrieved from 3D CFD computations. The second approach is preferred, as experimental data may not always be available and 3D CFD computation offer more information on the local flow details (Defoe *et al.*, 2010). However, it was observed in the present application that directly using the classical blade computations to extract the coefficients could lead to singular values of K_n due to its dependence on $1/\sin 2\delta$, which had already been reported by Peters *et al.* (2014). Peters' solution was to empirically modify the normal force expression so as to avoid spurious oscillations of K_n. In the present study, it was found that performing the calibration on RANS-extracted body forces computations allows to drastically decrease the number of singular values and to obtain better results and better convergence during the computations with Gong's model. The remaining singular values are eliminated by fitting K_n distributions as functions of the blade metal angle for each spanwise section.

The parallel force coefficient is decomposed in three coefficients, so as to form a loss bucket around the maximum efficiency point of the turbomachinery row. Several computations are thus necessary to calibrate the model. In the present case, these coefficients are computed using a second order fit on an overall speed line, whereas the

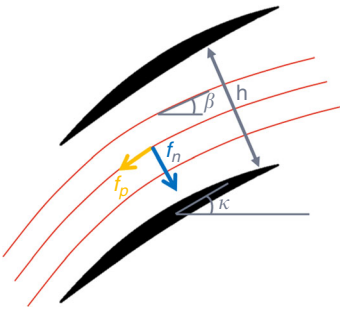

Figure 4.
Illustration of the normal and parallel force components in Gong's model

normal force coefficient is computed as the mean coefficient over the speed line. Each set of coefficients is thus valid only for one rotational speed and the model must be calibrated again to compute a different speed line.

3. Application

3.1 Geometry and numerical settings

The fan geometry is a nine inch wind-tunnel test fan designed for experimentation purposes, whose characteristics are summarized in Table I. The fan was meshed with NUMECA Autogrid and the body force grids were generated with NUMECA IGG.

CFD simulations are performed with the solver elsA (Cambier *et al.*, 2013), developed by Onera. Body force computations are realized in the framework of the flowsimulator environment (Meinel and Einarsson, 2010): the solver is coupled in-memory with a python module created for the purpose of this study, which generates source terms added to the right hand side of the RANS equations (Figure 5).

The RANS equations are solved in the rotating frame for the fan computations and in the absolute frame for body forces computations, using an implicit pseudo time-marching method. A V-cycle multigrid technique on three levels is used to improve convergence rate with the fan geometry, but body force computations are only performed on one grid level due to implementation limitations. The spatial discretization uses a cell-centered finite volume approach, and turbulence closure is achieved with the one equation turbulence model of Spalart and Allmaras (1994).

3.2 Isolated single passage computations

The two body force approaches are first assessed on isolated single passage computations. This step aims at evaluating the body force capability and calibrating the models for a given blade geometry.

3.2.1 Single passage mesh and operating conditions. The meshes used to perform the single passage computations are described in Figures 6 and 7. The body force mesh consists in a 3D axysimmetric mesh, the blade shape being taken into account by forcing mesh lines along the meridional leading edge and trailing edge curves. Compared to the fan grid, the body force grid has a much higher quality and a much lower number of mesh cells, as described in Table II. The low orthogonality in the fan

Table I.
Nine inch fan characteristics

Diameter	Blade number	Solidity (mid span)
0.23 m	21	1.66

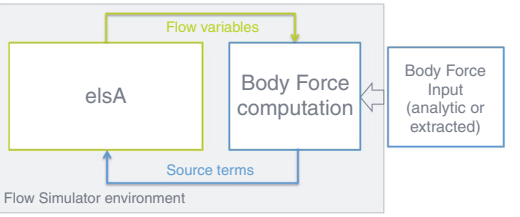

Figure 5.
Illustration of the coupling between the solver elsA and a python module in flowsimulator to generate source terms

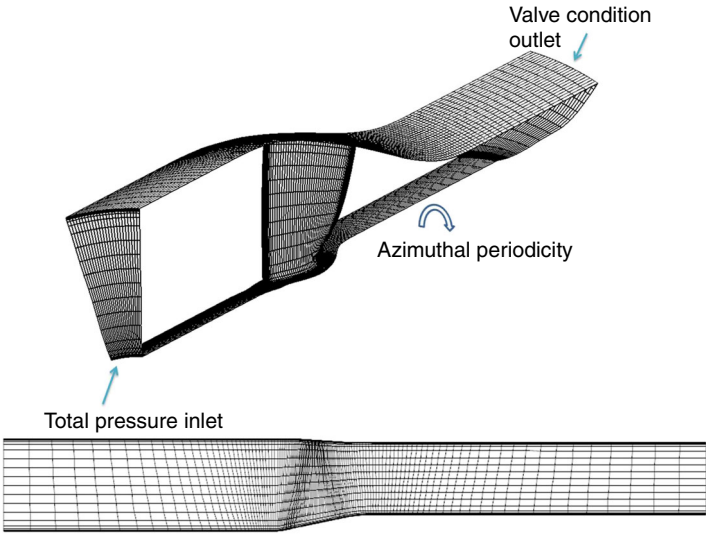

Note: One every two points shown

Figure 6.
Single passage fan mesh

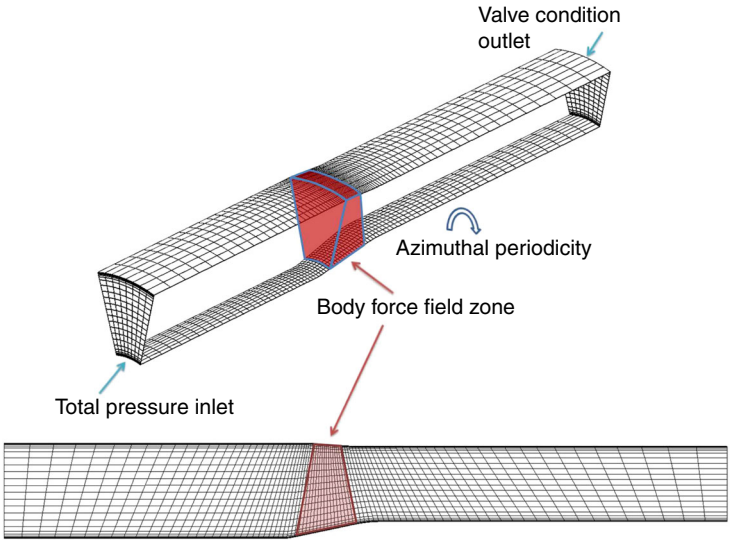

Note: One every two points shown

Figure 7.
Single passage body force mesh

	Fan	Body force
Number of cells	1,500 k	300 k
Min. orthogonality	15°	56°
Max. expansion ratio	1.9	1.3

Table II.
Mesh characteristics for single passage computations

mesh is due to the large fillet of the rotor, leading to highly curved mesh line in the spanwise direction near the hub.

To keep the same level of accuracy in the determination of the end walls boundary layer, the number of cells in the radial direction was set to the same value in both meshes, the only difference being due to the absence of the tip gap in the current body force implementation. The number of cells in the axial direction in the body force grid was set to a value equal to 33 between the leading and trailing edges.

In both cases, the total conditions are imposed at the inlet and a valve condition with radial equilibrium is imposed at the outlet. This boundary condition updates the outlet static pressure at each iteration according to following equation:

$$P(N+1) = P_{ref} + \omega\left(\frac{Q(N)}{Q_{ref}}\right)^2 \tag{10}$$

where Q denotes a mass flow and P a static pressure. For a given reference pressure and reference mass flow, changing the valve relaxation factor ω allows to compute different operating points along a speed line.

Blade computations are run for three different rotational speeds, and the procedures described in Sections 2.2.1 and 2.2.2 are applied to each operating points to extract body forces and calibrate Gong's model. The body force computations are performed with and without the blockage source term.

3.2.2 Single passage results. All the results are compared to the classical computations with the blade geometry. First, a global analysis of the compressor map (total pressure ratio and total temperature elevation) is proposed. Then, a local analysis is performed based on mass weighted pitch-averaged radial profiles extracted downstream of the rotor.

Metal blockage effect. As mentioned in Section 2.1, the present implementation of the blockage factor includes a source term in the density equation, which could lead to non-conservative mass flow across the blade row. The computations show differences between inlet and outlet mass flow with an average of 0.05 and up to 0.2 percent for the worst cases. A potential improvement might be to compute the blockage derivatives with a finite volume approach, more accurate, and more conservative compared to the finite difference method employed in this study. It was also observed that the blockage source term has a positive effect on the convergence of the body force solutions. For high rotational speed in particular, some operating points cannot converge without the blockage source term. More generally, more iterations are necessary to ensure convergence of any operating point without the blockage effects.

Figures 8 and 9 present the normalized total temperature elevation as a function of mass flow. They show that the blockage source term has a strong impact on the performance prediction of both body force approaches. Without the blockage source term, and the maximum mass flow are overestimated:

$$\frac{\partial h_t}{\partial m} = \Omega r \frac{F_\theta}{V_m} \tag{11}$$

where Ω is the rotational speed of the blade row and V_m the flow velocity in the meridional plane.

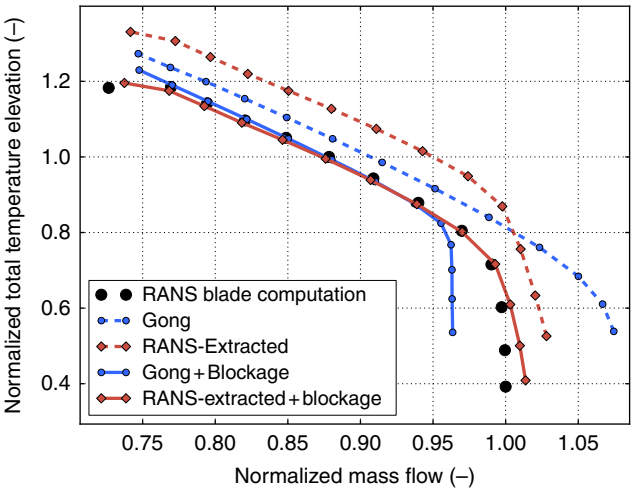

Figure 8.
Normalized total temperature elevation at 22,500 RPM, with and without the blockage term

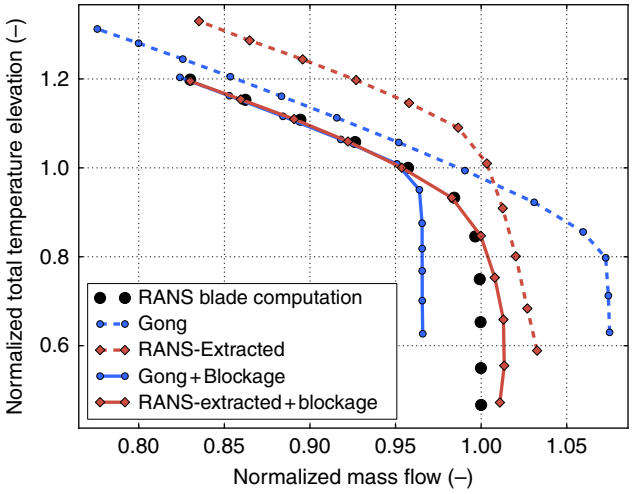

Figure 9.
Normalized total temperature elevation at 27,500 RPM, with and without the blockage term

With the blockage term, the work produced by the rotor is correctly captured by both body force methods, but discrepancies on the value of the choked mass flow are still present. Gong's model underestimates its value by about 3 percent, and the RANS-extracted body forces overestimates its value by about 1.5 percent (Table III). While this first discrepancy can be attributed to the construction of Gong's model, the latter is thought to be mainly resulting from the omission of the aerodynamic blockage effects due to the boundary layers on the blades.

Comparison of Gong's model and RANS-extracted body forces. Figures 10 and 11 show the performance map obtained with both approaches, including the metal blockage effect. It can be seen on these curves that while the two approaches capture the general performance of the fan quite well, the extracted body force methodology provides better

results, especially in the choked region of the characteristics. Figures 12-14 show radial profiles of the total pressure relative error between RANS blade computations and body force computations downstream of the rotor, extracted from mass-weighted pitch averaged solutions. The radial profiles of the two approaches agree very well to the

RPM	Gong (%)	Extr. (%)	Gong + b (%)	Extr. + b (%)
22,500	7.5	2.8	−3.6	1.4
27,500	7.5	3.3	−3.4	1.3
32,000	8.3	3.4	−1.4	1.4

Table III. Choked mass flow rate values

Note: Relative error on the maximum mass flow rate between the body force approaches and classical CFD computations

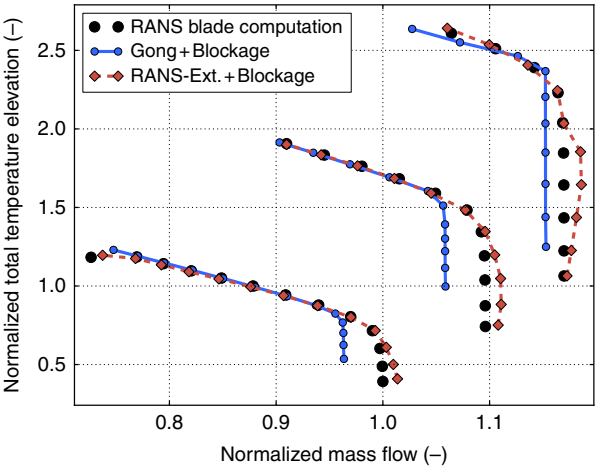

Figure 10. Fan performance map in terms of normalized total temperature elevation

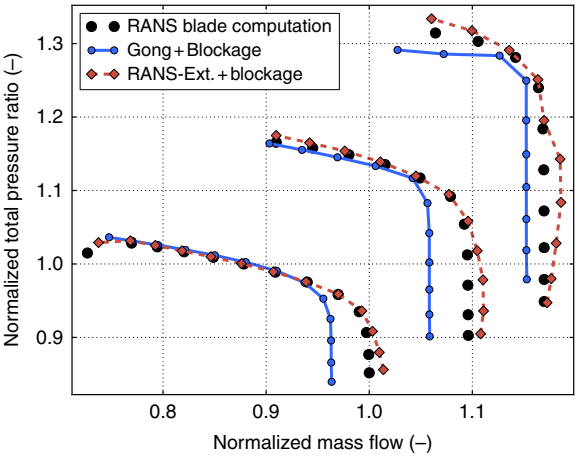

Figure 11. Fan performance map in terms of normalized total pressure ratio

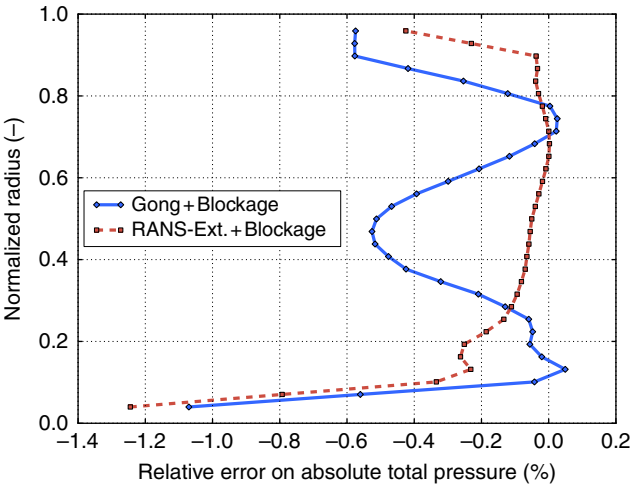

Figure 12.
Radial profile of the total pressure relative error at the fan trailing edge (22,500 RPM, $Q^* = 0.91$)

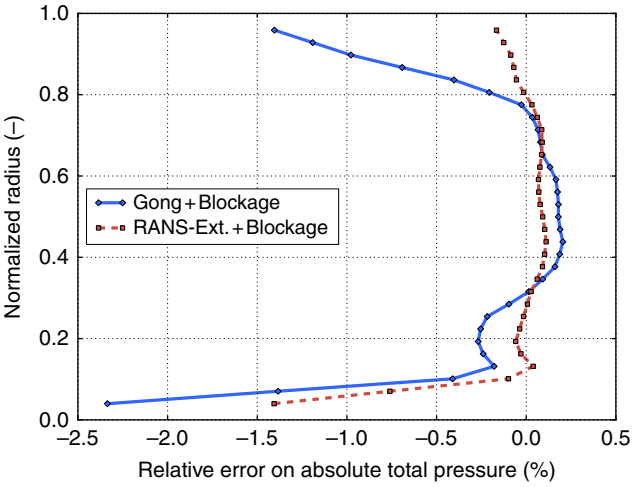

Figure 13.
Radial profile of the total pressure relative error at the fan trailing edge (27,500 RPM, $Q^* = 1.05$)

classical CFD profiles, with relative errors below 1.0 between 10 and 90 percent span at 22,500 and 27,500 RPM, and with a small degradation of Gong's model prediction at 32,000 RPM.

3.3 Air intake test case

The body force approach is assessed on an intake-engine integration test case. The fan geometry is placed inside an air intake, whose geometry is shown in Figure 15. A valve condition is imposed behind the fan and the rear part of the engine (pylon, bifurcation) is not represented.

3.3.1 URANS and body force methodologies for short intake application. Others numerical parameters remain as described in Section 3.1. To ensure a proper convergence of the unsteady computations, the following process is applied for each

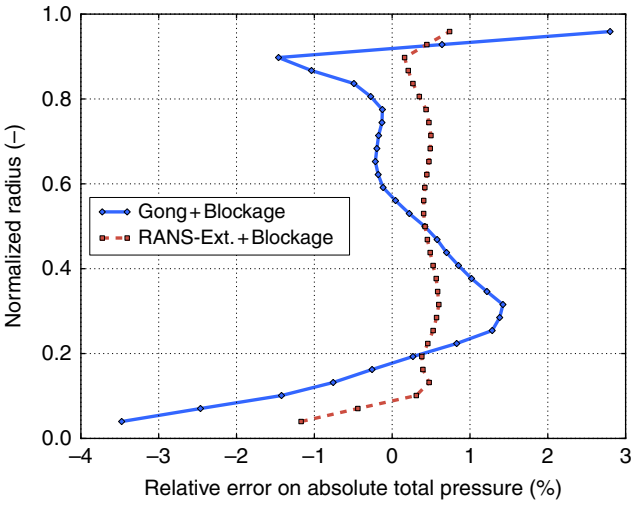

Figure 14.
Radial profile of the total pressure relative error at the fan trailing edge (32,000 RPM, $Q^* = 1.14$)

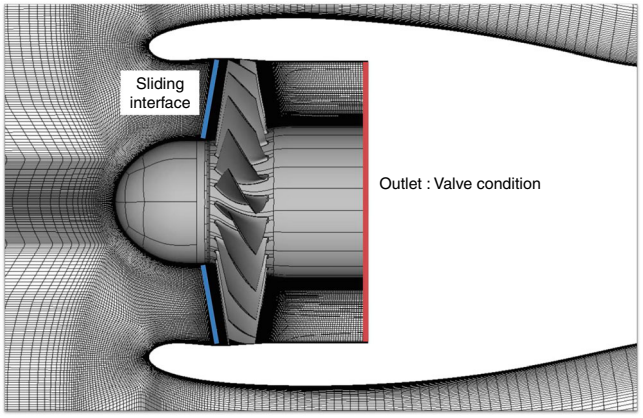

Figure 15.
Air intake and fan geometries

operating point. A first computation with one single blade passage inside the intake is performed, using a mixing plane at the interface (Denton, 1992). Then, the computed solution is duplicated on 360°. This full annulus solution is used to perform a first unsteady computation with a time step equivalent to ten time steps for one blade passage, for a total of five rotations. Then, the time step is reduced to 60 time steps by blade passage, and three more rotations are performed. Finally, one last rotation is performed and the flow is time averaged.

Body force computations can be performed directly on the full annulus, which removes the task of duplication of the solution for each operating point.

3.3.2 Air intake results. Unsteady and Gong's model results are compared to those obtained with an intake-only approach with no fan and no source terms. The comparison is done for similar mass flows, with less than 0.2 percent variations. Several operating points are computed with this method, representing low speed and

low altitude operating conditions, for increasing AOAs, until flow separation occurs on the intake lips. The chosen rotational speed is 27,500 RPM. As shown in Section 3.2.2, Gong's model is unable to capture the correct mass flow rate in the choked region of the map. It was therefore impossible to match the mass flow obtained in the URANS simulations with Gong's approach and the blockage term, for the same rotational speed. To address this, the rotational speed of those computations was increased until the good mass flow was obtained (30,000 RPM), at iso-valve coefficient at the outlet. While these computations converged correctly, it was impossible to reach convergence without the blockage term.

The circumferential distortion index defined in Equation (12), which measures the global heterogeneity of the flow in the tangential direction, is shown on Figures 16 and 17.

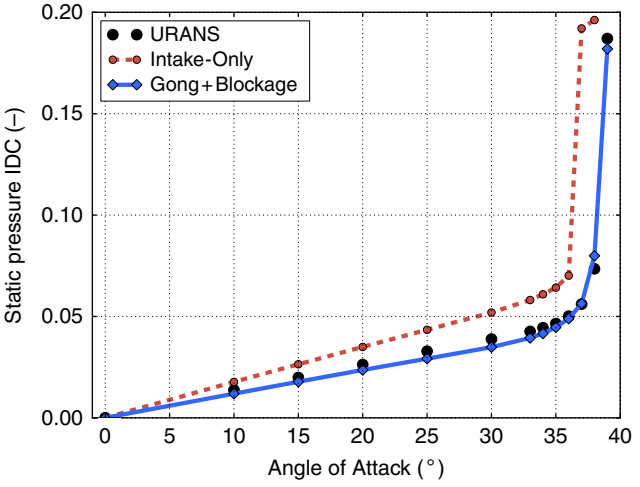

Figure 16.
Static pressure IDC evolution at the inlet-fan interface

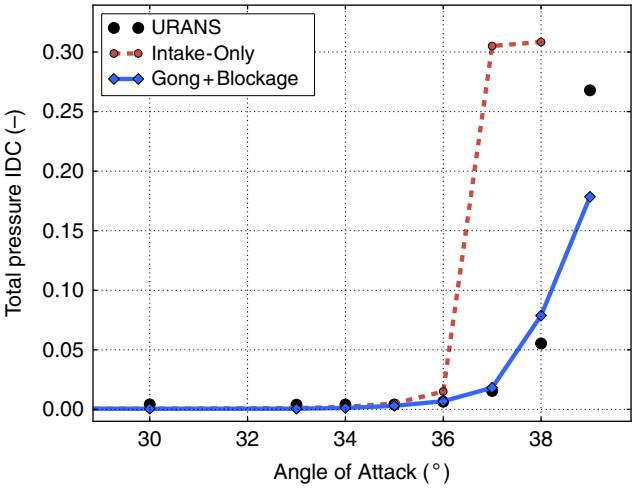

Figure 17.
Total pressure IDC evolution at the inlet-fan interface

The agreement between Gong's model and the reference URANS computation is very good for every values of the AOA. Gong's model captures both the fan effect on the upstream static pressure distortion and the fan effect on the AOA at which flow separation occurs, which is characterized by a strong augmentation of the total:

$$IDC = \max_{0 \leqslant i \leqslant n-1} 0.5\left(\frac{\overline{P}_i - P_{min_i} + \overline{P}_{i+1} - P_{min_{i+1}}}{\overline{P}}\right) \tag{12}$$

with n the number of radial positions (5); $\overline{P}$ the average pressure in the IDC plane; $\overline{P}_i$ the average pressure on the ith radius; and P_{min_i} the minimum pressure on the ith radius pressure IDC. This is to be compared to the nacelle-only computation, which confirms both the necessity of accounting for the fan and the relevance of the body force approach.

The circumferential evolution of the static pressure at 33° and 38° AOA at the inlet throat are shown in Figures 18 and 19. Gong's model reproduces accurately the mean effect of the fan on the inlet walls, again with an error largely inferior to the intake only case.

Figure 20 shows the upstream effect of the fan on the distortion, which is not captured in the intake-only approach, but quite well captured by Gong's model.

4. Conclusion

The applicability of two body force methods to the evaluation of aerodynamic interaction between an air intake and a fan has been investigated. An analytic model and RANS-extracted body forces were applied to an isolated fan test case. First, it was shown that taking into account the blockage effects with a source term allows to improve the prediction of the work produced by the fan as well as to improve the convergence of the body force computations. Then, the accuracy of the RANS-extracted body forces in terms of performance prediction was demonstrated.

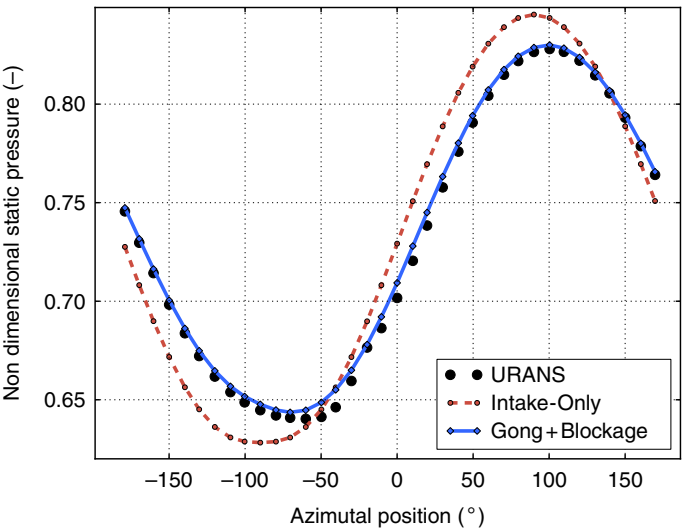

Figure 18.
Circumferential evolution of the non-dimensional static pressure on the inlet lips at the throat, AOA = 33°

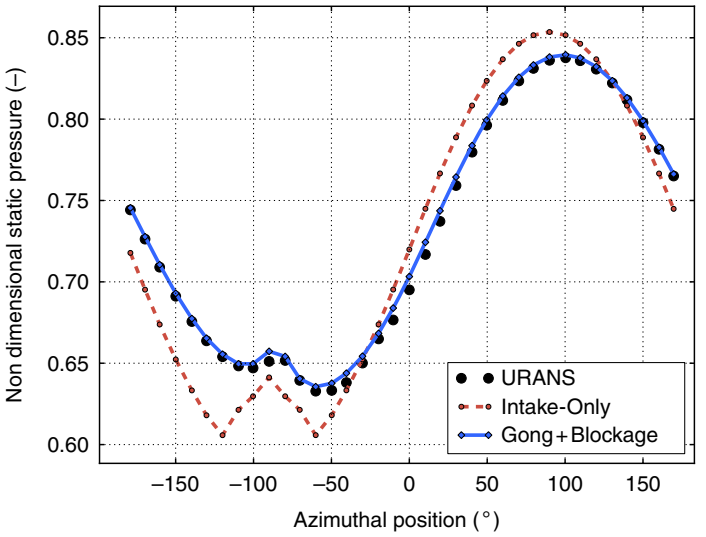

Figure 19.
Circumferential evolution of the non-dimensional static pressure on the inlet lips at the throat, AOA = 38°

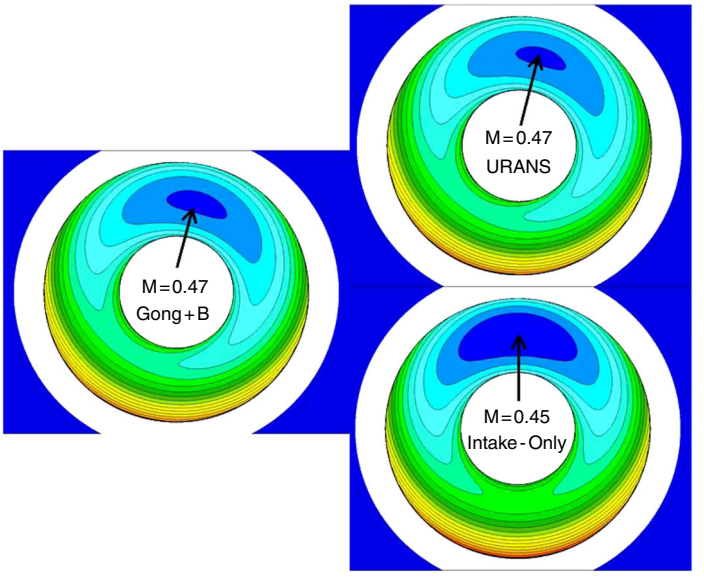

Note: The indicated mach number corresponds to the global minimum observed on this plane

Figure 20.
Mach number contours on the inlet throat plane, AOA = 33°

Finally, the analytic model was applied to an air intake test case, which shows the necessity to take into account the fan effects, and the relevance of the body force approach to capture these effects.

In this study, Gong's model was found to underestimate the choked mass flow of the fan considered. The model should therefore be modified in further work to correctly predict the fan behavior and enable the possibility of accurately capture the fan-intake

interactions, both in terms of fan performance and intake performance. Another promising approach is the development of an interpolation/extrapolation method that would allow to extend the RANS-extracted approach to any operating conditions and to non-axisymmetric cases.

References

Benneke, B. (2009), "A methodology for centrifugal compressor stability prediction", master's thesis, Massachusetts Institute of Technology, Cambridge, MA.

Cambier, L., Heib, S. and Plot, S. (2013), "The Onera elsA CFD software: input from research and feedback from industry", *Mechanics & Industry*, Vol. 14 No. 3, pp. 159-174.

Defoe, J., Narkaj, A. and Spakovszky, Z. (2010), "A body-force-based method for prediction of multiple-pure-tone noise: validation", *16th AIAA/CEAS Aeroacoustics Conference, Number 3747, Stockholm, June*.

Denton, J.D. (1992), "The calculation of three-dimensional viscous flow through multistage turbomachines", *Journal of Turbomachinery*, Vol. 114 No. 1, pp. 18-26.

Fidalgo, V.J., Hall, C.A. and Colin, Y. (2012), "A study of fan-distortion interaction within the NASA Rotor 67 transonic stage", *Journal of Turbomachinery*, Vol. 134 No. 5, pp. 1-12.

Gong, Y. (1998), "A computational model for rotating stall and inlet distortions in multistage compressors", PhD thesis, Massachusetts Institute of Technology, Cambridge, MA.

Hall, C.A. and Crichton, D. (2007), "Engine design studies for a silent aircraft", *Journal of Turbomachinery*, Vol. 129 No. 3, pp. 479-487.

Hsiao, E., Naimi, M., Lewis, J.P., Dalbey, K., Gong, Y. and Tan, C. (2001), "Actuator duct model of turbomachinery components for Powered-Nacelle Navier-Stokes calculations", *Journal of Propulsion and Power*, Vol. 17 No. 4, pp. 919-927.

Kiwada, G. (2008), "Development of a body force description for compressor stability assessment", master's thesis, Massachusetts Institute of Technology, Cambridge, MA.

Kottapalli, A.P. (2013), "Development of a body force model for centrifugal compressors", master's thesis, Massachusetts Institute of Technology, Cambridge, MA.

Larkin, M.J. and Schweiger, P.S. (1992), "Ultra high bypass nacelle aerodynamics: inlet flow-through nacelle high angle of attack distortion test", Technical Report No. 189149, NASA, East Hartford.

Marble, F. (1964), *Three Dimensional Flow in Turbomachines, Volume X of High Speed Aerodynamics and Jet Propulsion*, Princeton University Press, Princeton, pp. 83-166.

Meinel, M. and Einarsson, G.O. (2010), "The flowsimulator framework for massively parallel CFD applications", *PARA 2010 Conference: State of The Art in Scientific and Parallel Computing, Reykjavik, June*.

Owens, R., Hasel, K. and Mapes, D. (1990), "Ultra high bypass turbofan technologies for the twenty-first century", *26th Joint Propulsion Conference, Volume 1990-2397, AIAA, Orlando, July*.

Patel, A.A. (2009), "Assessment of a body force representation for compressor stability estimation", master's thesis, Massachusetts Institute of Technology, Cambridge, MA.

Peters, A., Spakovszky, Z.S., Lord, W.K. and Rose, B. (2014), "Ultra-short nacelles for low fan pressure ratio propulsors", *ASME, Journal of Turbomachinery*, Vol. 137 No. 2, pp. 021001-1-021001-14, doi: 10.1115/1.4028235

Spalart, P.R. and Allmaras, S.R. (1994), "A one-equation turbulence model for aerodynamic flows", *La Recherche Aérospatiale*, No. 1, pp. 5-21.

Simon, J.F. (2007), "Contribution to throughflow modelling for axial flow turbomachines", PhD thesis, Universite de Liege, Liège.

Yao, J., Gorrell, S.E. and Wadia, A.R. (2010), "High-fidelity numerical analysis of per-REV-type inlet distortion transfer in multistage fans – part 1: simulations with selected blade rows", *ASME Journal of Turbomachinery*, Vol. 132 No. 4, pp. 041014-1-041014-10, doi: 10.1115/1.3148478

Further reading

Fillola, G., Le Pape, M.-C. and Montagnac, M. (2004), "Numerical simulations around wing control surfaces", *24th International Congress of the Aeronautical Sciences, ICAS, Yokohama, August-September*.

Gourdain, N., Montagnac, M., Wlassow, F. and Gazaix, M. (2010), "High-performance computing to simulate largescale industrial flows in multistage compressors", *International Journal of High Performance Computing Applications*, Vol. 24 No. 4, pp. 429-443.

Corresponding author

William Thollet can be contacted at: william.thollet@airbus.com